

Fall 11-9-2012

Influence of Line Tension on Spherical Colloidal Particles at Liquid-Vapor Interfaces

Sean P. McBride

Marshall University, mcbrides@marshall.edu

Bruce M. Law

Follow this and additional works at: http://mds.marshall.edu/physics_faculty



Part of the [Physics Commons](#)

Recommended Citation

McBride, S. P.; Law, B. M. Influence of line tension on spherical colloidal particles at liquid-vapor interfaces. *Phys. Rev. Lett.* 2012, 109, 196101, DOI: 10.1103/PhysRevLett.109.196101

This Article is brought to you for free and open access by the Physics at Marshall Digital Scholar. It has been accepted for inclusion in Physics Faculty Research by an authorized administrator of Marshall Digital Scholar. For more information, please contact zhangj@marshall.edu, martj@marshall.edu.

Influence of Line Tension on Spherical Colloidal Particles at Liquid-Vapor Interfaces

Sean P. McBride and Bruce M. Law*

Physics Department, Kansas State University, 116 Cardwell Hall, Manhattan, Kansas 66506 2601, USA
(Received 27 March 2012; published 7 November 2012)

Atomic force microscopy (AFM) imaging of isolated submicron dodecyltrichlorosilane coated silica spheres, immobilized at the liquid polystyrene- (PS-) air interface at the PS glass transition temperature, T_g , allows for determination of the contact angle θ versus particle radius R . At T_g , all θ versus R measurements are well described by the modified Young's equation for a line tension $\tau = 0.93$ nN. The AFM measurements are also consistent with a minimum contact angle θ_{\min} and minimum radius R_{\min} , below which single isolated silica spheres cannot exist at the PS-air interface.

DOI: [10.1103/PhysRevLett.109.196101](https://doi.org/10.1103/PhysRevLett.109.196101)

PACS numbers: 68.37.Ps, 61.46.Df, 68.03.Cd, 68.08.Bc

Line tension is due to an excess of energy caused by the imbalance of intermolecular forces at the three phase contact line (TPCL) [1]. This TPCL exists in systems (1) where liquid droplets reside on solid-vapor or liquid-liquid interfaces or (2) when solid particles reside on liquid-liquid or liquid-vapor interfaces (LVIs). The line tension, τ , or energy per unit length associated with this TPCL [2] is a subject of continuing interest [3–6]. Line tensions for liquid droplets have been measured on both liquid [7] and solid interfaces [8–10] and for spherical colloids at liquid interfaces [5,11–14]. The line tension has been shown to influence the surface nucleation of liquid droplets [15], the surface aggregation and fragmentation dynamics of liquid droplets with liquid droplets [7], the wettability of liquid droplets in the vicinity of a wetting transition [8,16], and the stability of films and foams [17], and is expected to play a significant role in particle self-assembly at liquid interfaces [18].

Understanding the line tension τ will be important to a range of industrial and scientific processes that involve submicron particles at liquid interfaces including the emulsification of cleaner liquid fuels [19], nanoparticle catalysis for biofuel production [20], targeted drug delivery processes [21–23], and nanoparticle membranes which self-assemble at liquid interfaces [5,18,24]. As the interfacial particle size decreases, τ will play an increasingly important role in the stability of such systems [25,26]. The sign of τ determines whether the contact angle θ , associated with the TPCL at the LVI, decreases or increases with increasing size where both signs have been measured [2,3,25]. The experimental magnitude for τ varies considerably (10^{-12} to 10^{-6} N) where some measurements agree with theoretical expectations ($\tau \sim 10^{-12}$ to 10^{-10} N) [2,27,28], while many others are orders of magnitude larger than theoretical expectations [3,5,25,29]. The magnitude of τ is a controversial subject, and the source of discrepancies between theory and experiment has yet to be resolved.

In this work, we investigate τ for submicron particles at LVIs. For these systems, there are a number of unresolved

problems. How can one reliably determine θ for submicron particles at liquid interfaces [30,31] and what role does τ play in determining the surface properties of particles at this interface [5]? Does τ influence the phase behavior of particles at this interface and at what size scale does this effect become important [32]? In this Letter, we answer all of these questions using a novel technique for studying particles at the polymer-air interface. Unlike existing techniques [3–6], the innovative technique used here takes advantage of the high topographical resolution available in atomic force microscopy (AFM). Our experimental technique requires particles to be first equilibrated at a temperature well above the glass transition temperature, T_g , of the polymer (liquid phase), then allowed to cool slowly below T_g (solid phase). Atomic force microscopy is used at room temperature to image particles (of radius R) embedded at this solidified polymer interface, allowing accurate determination of the particle contact angle θ at T_g . The line tension τ is determined by comparing the modified Young's equation [Eq. (4)] with θ versus R data. These observations provide significant insights into particle phase behavior and self-assembly at the LVI.

In the experiments, polystyrene (PS) samples containing silica spheres with radii $R \sim 88$ –498 nm (Table I), at typical concentrations of ~ 2 –8 wt%, were prepared as follows. The silica spheres, acquired from Particle Solutions LLC, Bang Laboratories, or grown via the Stöber method [33] were first cleaned [34] and then coated with dodecyltrichlorosilane using wet chemistry [34,35]. In the Stöber method, the silica sphere radius was controlled by the amount of ammonium hydroxide NH_4OH (0.71–1.3 mL) added to a tetraethylorthosilicate ethanol solution [33,34]. Several milliliters of a chloroform + silica particle stock solution (100 mg coated spheres to 10 μL chloroform) was mixed with ~ 30 mg of PS by sonication. Chloroform was evaporated off via periodic heating and sonication. This mixture was deposited onto a hydrofluoric acid glass etched microscope slide. Residual chloroform (boiling point $\sim 61^\circ\text{C}$) was completely removed by heating the sample above T_g to 100°C for 12 hours in an enclosed

TABLE I. Average PS-silica sphere sample characteristics (# = number of experimental measurements).

	(#)	R_o (nm)	(#)	R (nm)	b (nm)	h (nm)	θ (deg.)
Bangs Lab. Inc.	34	518	15	498	440	267	62.3
Bangs Lab. Inc.	51	248	20	265	238	150	64.2
Stöber(1.3 mL)	34	184	12	197	167	93	58.0
Stöber(1.7 mL)	19	144	20	147	124	69	57.8
Stöber(0.9 mL)	30	125	5	139	118	67	56.6
Stöber(0.8 mL)	41	114	5	130	107	57	55.9
Stöber(0.77 mL)	41	96	16	122	101	54	56.2
Stöber(0.766 mL)	53	85	11	115	93	48	54.7
Stöber(0.762 mL)	46	66	9	116	88	43	53.8
Stöber(0.71 mL)	473	66	16	98	76	35	49.7
Particle Sol. LLC.	131	67	18	88	57	19	38.8

environment. The chloroform free sample was cooled to T_g naturally over many hours, thus “freezing” in the liquid equilibrium state of the particles at the LVI. The PS, from Polymer Standards Service, Mainz, Germany, has a molecular weight $MW \sim 1890 \text{ g} \cdot \text{mol}^{-1}$, polydispersity index ~ 1.06 , glass transition temperature $T_g \sim 46.9^\circ\text{C}$ [36], and surface tension $\gamma_{LV} \approx 39.9 \pm 0.5 \text{ mN/m}$ at T_g [34]. The PS macroscopic contact angle, on a molecularly smooth dodecyltrichlorosilane coated Si wafer, is $\theta_\infty \approx 64.8 \pm 1.0^\circ$. Both γ_{LV} and θ_∞ were measured using a long range microscope (First Ten Angstroms FTA100) [34].

An Asylum Research MFP-3D AFM with an Olympus AC240TS cantilever (tip radius $\sim 9 \pm 2 \text{ nN}$) was used for imaging. Isolated spheres, at least 10 sphere diameters from any neighbors, were imaged and the lateral radius b and protrusion height h [defined in the Fig. 2(b) inset] were measured using the AFM amplitude and height trace, respectively (Fig 1 inset). The lateral radius b was extracted from the amplitude trace by fitting a circle to 16 points placed at the TPCL using Image Pro Plus 5.0 software. The particle radius R and contact angle θ (Fig. 1) were determined from b and h using the geometric relationships $R = (b^2 + h^2)/2h$ and $\theta = \cos^{-1}(1 - h/R)$. The measurement uncertainties in b and h are estimated to be $\Delta b = \pm 11 \text{ nm}$ (worst case tip sharpness) and $\Delta h = \pm 0.01R$. Any AFM images which exhibited nano-scale contamination or TPCL pinning in the phase or amplitude trace images were excluded from consideration [34]. Pure solidified PS, with no nanospheres present exhibited a surface roughness comparable to a silicon wafer [34].

The R versus θ data in Fig. 1 can be understood by considering the particle energy at the LVI,

$$E_s = \gamma_{SV}A_1 + \gamma_{SL}A_2 + 2\pi b\tau, \quad (1)$$

where γ_{ij} is the surface energy between phases i and j (S , L , and V denote solid, liquid, and vapor, respectively), A_1

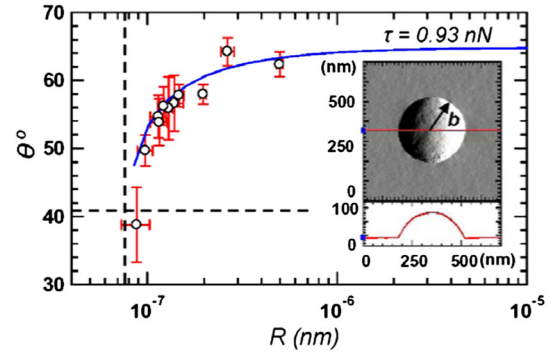


FIG. 1 (color online). Contact angle θ versus particle radius R . Group averaged experimental data (symbols), modified Young's equation Eq. (4) for $\tau = 0.93 \text{ nN}$ (solid line), θ_{\min} Eq. (5), (horizontal line), R_{\min} Eq. (6), vertical line. Inset: AFM amplitude (upper) and height trace (lower) for Stöber $R \sim 184 \text{ nm}$ silica sphere.

(A_2) is the upper (lower) spherical cap area, while τ is the line tension associated with the TPCL of length $2\pi b$. Energy for particle attachment to this interface is obtained by comparing E_s with the energy of a completely submerged particle [25],

$$E_b = \gamma_{SL}(A_1 + A_2) + \pi b^2 \gamma_{LV}. \quad (2)$$

When the particle is submerged, Eq. (2) accounts for the extra LVI surface area of size πb^2 now present with surface energy γ_{LV} . Geometry requires that $b = R \sin\theta$, $h = R(1 - \cos\theta)$, and $A_1 = 2\pi R h$; hence the attachment energy $E = E_s - E_b$ becomes [37].

$$E = \gamma_{LV} \cos\theta_\infty 2\pi R^2 (1 - \cos\theta) + \tau 2\pi R \sin\theta - \gamma_{LV} \pi R^2 \sin^2\theta, \quad (3)$$

where Young's equation [38], $\cos\theta_\infty = (\gamma_{SV} - \gamma_{SL})/\gamma_{LV}$, has been used. Here, θ_∞ is the macroscopic contact angle the liquid would make with an infinitely large particle (i.e., $R \rightarrow \infty$) or, equivalently, the contact angle the liquid makes with a molecularly smooth flat solid surface possessing identical surface chemistry to the particle. The particle is in mechanical equilibrium at the LVI, hence $(dE/d\theta) = 0$ which gives rise to the modified Young's equation [11,32,37]

$$\cos\theta = \cos\theta_\infty [1 - \tau/b\gamma_{LV}]^{-1}. \quad (4)$$

This equation describes how θ varies as a function of particle radius R due to the presence of τ . This energy minimum, $(d^2E/d\theta^2) > 0$, disappears when $(d^2E/d\theta^2)|_{\theta_{\min}} = 0$ (i.e., at a saddle point) implying that there is a minimum angle θ_{\min} , below which single isolated particles can no longer exist at the LVI where [11,32,37,39]

$$\cos\theta_{\min} = [\cos\theta_\infty]^{1/3}. \quad (5)$$

Equations (4) and (5) imply that there is a minimum radius R_{\min} given by

$$R_{\min} = \tau[\gamma_{LV} \sin\theta_{\min}(1 - \cos\theta_{\infty}/\cos\theta_{\min})]^{-1}, \quad (6)$$

below which single particles are unstable at the LVI and these particles are submerged into the bulk liquid phase. Equations (1)–(6) describe the physics of isolated particles at a LVI. They predict that θ should obey Eq. (4) and that no isolated particles should exist at the LVI if $\theta < \theta_{\min}$ or $R < R_{\min}$. Equation (6) also implies a change in the interfacial phase behavior when $R < R_{\min}$, namely, a gaseous phase of (single isolated) particles can no longer coexist with clusters of particles. These equations however make no statement about the behavior of particles within a surface cluster; hence, particles within a cluster could potentially possess $\theta < \theta_{\min}$ or $R < R_{\min}$.

Figure 1 and Table I summarize average θ versus R measurements determined from 147 individual spheres grouped into 11 size ranges with radii varying from $R \sim 88$ to 498 nm, where the error bars represent the standard deviation in experimental results. A nonlinear least squares fit of Eq. (4) to the 147 measurements yields $\tau = 0.93 \pm 0.01$ nN (Fig. 1, solid line). The horizontal and vertical dashed lines in Fig. 1 represent $\theta_{\min} \approx 40.4^\circ$ and $R_{\min} \approx 78$ nm, respectively, deduced from Eqs. (5) and (6) using the worst case measurement uncertainties; hence, our experimental θ and R data are self-consistent with these theoretical minima for θ_{\min} and R_{\min} .

In order to provide a better understanding of the colloidal particle attachment energy, E/kT [Eq. (3)] has been plotted as a function of R and θ in Fig. 2(a) where kT is the thermal energy and $\gamma_{LV} \approx 39.9 \pm 0.5$ mN/m, $\theta_{\infty} \approx 64.8 \pm 1.0^\circ$, and $\tau = 0.93$ nN are derived from our experiments. The heavy solid line on this plot represents the modified Young's equation energy minimum, Eq. (4). Cross-sections of E/kT versus θ , at fixed R , are provided in Fig. 2(b). The modified Young's equation minimum, occurs at $\theta \sim 1$ radian [$\theta \sim 41.2 \rightarrow 64.8^\circ$ as R increases from R_{\min} to ∞]. For $R > 124$ nm this minimum is a global minimum and possesses a lower energy than the energy minimum at $\theta = 0$. For $81.6 \text{ nm} < R < 124.0$ nm the “modified Young's minimum” is a local minimum and possesses a higher energy than the energy minimum at $\theta = 0$; however, particles at the LVI are kinetically trapped in this local minimum because there is an energy barrier ($\gg kT$) which separates the modified Young's minimum from the global minimum at $\theta = 0$. At $R_{\min} = 81.6$ nm [Eq. (6)] and $\theta_{\min} = 41.2^\circ$ [Eq. (5)] the modified Young's minimum disappears [heavy solid line, Fig. 2(b)] and the energy E exhibits a saddle point; single particles with $R < R_{\min}$ can no longer be found at the LVI, they acquire $\theta = 0$ and are completely wetted by the liquid (i.e., submerged beneath the liquid interface). These considerations hold provided that surface tension forces dominate gravitational forces, namely, $R \ll \kappa^{-1} = \sqrt{\gamma_{LV}/\rho g}$ where κ^{-1} , ρ , and g are the capillary length, liquid density, and acceleration due to gravity, respectively [40].

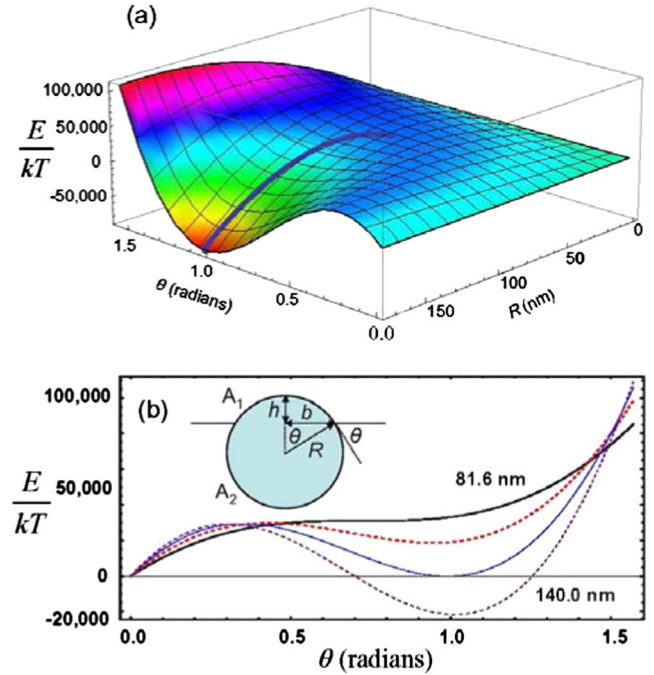


FIG. 2 (color online). (a) Particle attachment energy E/kT Eq. (3) for $\gamma_{LV} = 39.9$ mN/m, $\theta_{\infty} = 64.8^\circ$, and $\tau = 0.93$ nN. Modified Young's equation Eq. (4), solid line. (b) Energy cross-sections at fixed $R = 81.6, 105.0, 124.0$ and 140.0 nm where $R_{\min} = 81.6$ nm Eq. (6), heavy solid line. Inset: Schematic of spherical particle at a surface: protrusion height h , lateral radius b , contact angle θ , particle radius R , upper (lower) spherical cap area A_1 (A_2).

In Table I and Fig. 3(a) the “as-prepared” group averaged colloidal radius (R_o), measured via transmission electron microscopy (TEM, Philips CM-100), is compared with the group averaged colloidal radius (R) at the PS-air surface, measured via AFM. These two measures of R agree well, except for particles with $R < 130$ nm. This disagreement arises from the fact that the as-prepared distribution measured via TEM includes all particle sizes in a sample, whereas, the surface distribution measured via AFM includes only single (isolated) spheres at the PS interface with $R > R_{\min}$. As further evidence for the existence of $R_{\min} \sim 80$ nm, Fig. 3(d) compares a plot of the as-prepared (shaded and black line) and surface (white) normalized number distributions of spheres measured by TEM and AFM, respectively, from the same Stöber batch (0.71 mL NH_4OH) where the AFM (TEM) image is shown in Fig. 3(b) [Fig. 3(c)]. The as-prepared average radius $R_o \sim 66$ nm in Fig. 3(d) is below R_{\min} and only a small percentage of particles ($\sim 12\%$) lie above R_{\min} . By contrast, the PS-air distribution made from this same Stöber batch, but at very high silica particle concentration in PS (~ 20 wt%), is markedly skewed relative to the as-prepared sample where the surface distribution now starts around R_{\min} and only spheres with $R > R_{\min}$ are found at the PS interface. It is important to note that the surface

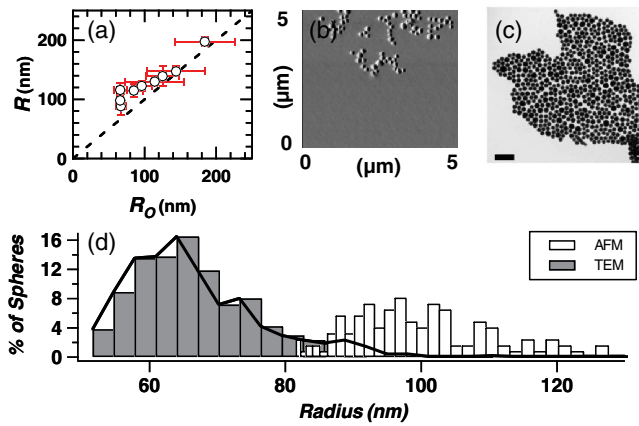


FIG. 3 (color online). Particle characteristics. (a) Average particle radii comparison: as-prepared sample measured via TEM (R_o), surface sample measured via AFM (R), dashed line of slope 1 if agreement is exact. (b) AFM image of Stöber silica spheres at PS-air interface. (c) TEM image of silica spheres (same Stöber batch, average radius $R_o \sim 66$ nm), scale bar = 500 nm. (d) Percentage sample distribution versus sphere radius R : as-prepared distribution (shaded rectangles + black line from 473 spheres measured using TEM), surface distribution (white rectangles from 123 spheres measured from two AFM images).

distribution displayed in Fig. 3(d) includes all particles shown in Fig. 3(b), both those in clusters as well as single isolated spheres; this should be contrasted with the data in Fig. 1, which represented only single isolated spheres at the PS-air interface. Equations (1)–(6) do not preclude the existence of small spheres with $R < R_{\min}$ within clusters; however, surprisingly the surface distribution exhibited in Fig. 3(d) contain no spheres with radii below R_{\min} , even within clusters. The most probable explanation for this observation lies in our preparation method. The silica spheres in PS are sonicated at high temperature, well above T_g ; this process is expected to physically separate smaller spheres from their supporting (surface) cluster, causing spheres with $R < R_{\min}$ to be submerged below the PS interface. Once the particles are submerged within the bulk polystyrene, no TPCL is present; therefore, surface tension forces no longer dominate and the particles will start to settle to the bottom of the PS sample (as the sphere's gravitational potential energy dominates its thermal energy for the current sphere size range [14]).

In summary, we have developed a novel technique which allows for the determination of θ at the LVI for any sized particle (from micrometers down to nanometers) at the glass transition temperature of a polymer. The particle protrusion height h , above the solidified polymer interface, and lateral radius b are measured via AFM. The accuracy of this method is only limited by the sharpness of the AFM tip. We have tested this method for dodecyltrichlorosilane coated silica spheres embedded in a solidified polystyrene-air interface and confirmed that the variation of θ with R is in excellent agreement with the modified Young's equation

[Eq. (4), Fig. 1] from which $\tau = 0.93 \pm 0.01$ nN is determined. Additionally, the surface averaged particle radius R (measured by AFM) agrees well with the averaged sample radius R_o (measured by TEM), except at very small R approaching R_{\min} [Fig. 3(a)]. Our AFM measurements are consistent with the existence of a θ_{\min} [Eq. (5)] and R_{\min} [Eq. (6)], below which individual isolated spheres cannot exist at the LVI [Figs. 1 and 3(d)]. The presence of a θ_{\min} and R_{\min} , which ultimately arises from the line tension τ , implies that the particle surface phase diagram changes when $R < R_{\min}$. At small R below R_{\min} , particle phase coexistence can no longer exist; namely, a particle cluster phase cannot coexist with a (single particle) gaseous phase as the latter phase is unstable.

The magnitude of the line tension τ is controversial. Some experiments have found agreement with theoretical expectations (where $\tau \sim 10^{-12}$ to 10^{-10} N) while others have determined τ values which may be orders of magnitude larger. Limitations in optical determinations of τ have been suggested as a potential source for these differences [40]. These limitations are not applicable to the current AFM based experiments where $\tau = 0.93$ nN is still an order of magnitude larger than theoretical expectations. Our belief, and the belief of other scientists [3,11,17], is that the distribution in τ values is more a measure of nature's spread in τ rather than necessarily a failing in experimental technique. For example, if the ligand coating the particle is similar in chemical structure to the liquid solvent, then one would expect a small τ value. Indeed this is what was found for dodecanethiol ligated gold nanoparticles at the LVI of a number of n -alkane solvents ($\tau \sim 1$ pN) [14]. By contrast, if the ligand coating the particle is dissimilar in chemical structure to the liquid solvent then one might expect a much larger τ ; this is the case in these current AFM-based measurements. The alkane-like dodecyltrichlorosilane ligand coating the particles is dissimilar to the polystyrene solvent, $[\text{C}_8\text{H}_8]_n$, and correspondingly a much larger line tension is found ($\tau \sim 1$ nN).

A potential explanation for the discrepancy between theoretical predications and a number of experiments can be found in the work of Huang and coworkers [41]. They demonstrated experimentally that the outermost subgroup of a molecule at the LVI predominantly determines the surface tension of a liquid. By analogy, it seems likely that the outermost subgroup of a molecule immediately in contact with the TPCL will predominantly determine τ for a system. This submolecular contact will be highly dependent upon the molecular structure of the ligand and the solvent, as well as their relative orientations. In general, this submolecular contact is poorly modeled in simulations and theories of τ , which primarily are adept at capturing the contributions to τ further from the TPCL.

The authors thank Professor Dr. Stephan Herminghaus and Professor Dr. Ralf Seemann for the polystyrene. The authors are also grateful for the gift of silica spheres (Lot

No. 101008-1) produced by Particles Solutions, LLC and distributed by Fiber Optic Center, Inc. The authors thank members of the NSF NIRT group at Kansas State University for useful comments. This research was funded by NSF Grants No. DMR-0603144 and No. CTS-0609318.

*bmlaw@phys.ksu.edu

- [1] J. W. Gibbs, *The Scientific Papers of J. Willard Gibbs* (Ox Bow Press, Connecticut, 1961), Vol. 1.
- [2] J. S. Rowlinson and B. Widom, *Molecular Theory of Capillarity* (Dover, New York, 2002).
- [3] A. Amirfazli and A. W. Neumann, *Adv. Colloid Interface Sci.* **110**, 121 (2004).
- [4] A. V. Nguyen and H. J. Schulze, *Colloidal Science of Flotation* (Marcel Dekker, Inc., New York, 2004), Vol. 118.
- [5] F. Bresme and M. Oettel, *J. Phys. Condens. Matter* **19**, 413101 (2007).
- [6] M. E. Flatte, A. A. Kornyshev, and M. Urbakh, *J. Phys. Condens. Matter* **20**, 073102 (2008).
- [7] Y. Ushijima, B. Ushijima, E. Ohtomi, Y. Takata, T. Takiue, M. Aratono, and H. Matsubara, *Colloids Surf., A* **390**, 33 (2011).
- [8] J. Y. Wang, S. Betelu, and B. M. Law, *Phys. Rev. Lett.* **83**, 3677 (1999).
- [9] T. Pompe and S. Herminghaus, *Phys. Rev. Lett.* **85**, 1930 (2000).
- [10] J. K. Berg, C. M. Weber, and H. Riegler, *Phys. Rev. Lett.* **105**, 076103 (2010).
- [11] A. Scheludko, B. V. Toshev, and D. T. Bojadjiev, *J. Chem. Soc. Faraday Trans. 1* **72**, 2815 (1976).
- [12] G. Gillies, M. Kappl, and H.-J. Butt, *Langmuir* **21**, 5882 (2005).
- [13] L. N. Arnaudov, O. J. Cayre, M. A. Cohen Stuart, S. D. Stoyanov, and V. N. Paunov, *Phys. Chem. Chem. Phys.* **12**, 328 (2010).
- [14] H. S. Wi, S. Cingarapu, K. Klabunde, and B. M. Law, *Langmuir* **27**, 9979 (2011).
- [15] B. M. Law, *Phys. Rev. Lett.* **72**, 1698 (1994).
- [16] J. O. Indekeu, *Int. J. Mod. Phys. B* **08**, 309 (1994).
- [17] R. Aveyard and J. H. Clint, *J. Chem. Soc., Faraday Trans.* **91**, 2681 (1995).
- [18] R. Krishnaswamy and A. K. Sood, *J. Mater. Chem.* **20**, 3539 (2010).
- [19] V. B. Menon, R. Nagarajan, and D. T. Wasan, *Sep. Sci. Technol.* **22**, 2295 (1987).
- [20] S. Crossley, J. Faria, M. Shen, and D. E. Resasco, *Science* **327**, 68 (2010).
- [21] P. Shah, D. Bhalodia, and P. Shelat, *Syst. Rev. Pharm.* **1**, 24 (2010).
- [22] D. J. Irvine, *Nature Mater.* **10**, 342 (2011).
- [23] H. Xin, X. Jiang, J. Giu, X. Sha, L. Chen, K. Law, Y. Chen, X. Wang, Y. Jiang, and X. Fang, *Biomaterials* **32**, 4293 (2011).
- [24] J. He, X.-M. Lin, H. Chan, L. Vuković, P. Král, and H. M. Jaeger, *Nano Lett.* **11**, 2430 (2011).
- [25] J. Drelich, *Colloids Surf., A* **116**, 43 (1996).
- [26] M. Zeng, J. Mi, and C. Zhong, *Phys. Chem. Chem. Phys.* **13**, 3932 (2011).
- [27] F. Bresme and N. Quirke, *Phys. Rev. Lett.* **80**, 3791 (1998).
- [28] H. Dobbs, *Langmuir* **15**, 2586 (1999).
- [29] V. G. Babak, *Rev. Chem. Eng.* **15**, 157 (1999).
- [30] A. Deák, E. Hild, A. L. Kovács, and Z. Hórvölgyi, *Phys. Chem. Chem. Phys.* **9**, 6359 (2007).
- [31] D. O. Grigoriev, J. Krägel, V. Dutschk, R. Miller, and H. Möhwald, *Phys. Chem. Chem. Phys.* **9**, 6447 (2007).
- [32] R. Aveyard and J. H. Clint, *J. Chem. Soc., Faraday Trans.* **92**, 85 (1996).
- [33] B. N. Khlebustov, V. Khanadeev, and N. Khlebustov, *Langmuir* **24**, 8964 (2008).
- [34] S. P. McBride, Ph.D. dissertation, Kansas State University, 2012, <http://hdl.handle.net/2097/13459>.
- [35] S. P. McBride and B. M. Law, *Rev. Sci. Instrum.* **81**, 113703 (2010).
- [36] T. G. Fox and P. J. Flory, *J. Appl. Phys.* **21**, 581 (1950).
- [37] R. Aveyard, B. P. Binks, and J. H. Clint, *Adv. Colloid Interface Sci.* **100–102**, 503 (2003).
- [38] J. N. Israelachvili, *Intermolecular and Surface Forces* (Academic, New York, 1992), 2nd ed.
- [39] The calculations in Refs. [32,37] are in $E - \theta - \tau$ subspace at constant radius R whereas, for our experiments, we are in $E - \theta - R$ subspace at constant τ (in Fig. 1 we vary R at constant temperature T_g). In either subspace, a saddle point occurs when both $dE/d\theta = 0$ and $d^2E/d\theta^2 = 0$ are obeyed, which leads to Eq. (5).
- [40] P.-G. De Gennes, F. Brochard-Wyart, and D. Quere, *Capillarity and Wetting Phenomena* (Springer-Verlag, Berlin, 2004).
- [41] P. Mach, C. C. Huang, and H. T. Nguyen, *Phys. Rev. Lett.* **80**, 732 (1998).